Agricultural Water Management 242 (2020) 106420

Contents lists available at ScienceDirect

Agricultural Water Management

journal homepage: www.elsevier.com/locate/agwat

Dynamic assessment of the impacts of global warming on nitrate losses from a subsurface-drained rainfed-canola field

Farzad Haghnazari[a], Fatemeh Karandish[a,b,*], Abdullah Darzi-Naftchali[c], Jiří Šimůnek[d]

[a] Water Engineering Department, University of Zabol, Zabol, Iran
[b] Twente Water Centre, University of Twente, P.O. Box 217, 7500AE Enschede, the Netherlands
[c] Water Engineering Department, Sari Agricultural Sciences and Natural Resources University, Sari, Iran
[d] Department of Environmental Sciences, University of California Riverside, Riverside, CA 92521, USA

ARTICLE INFO

Keywords:
HYDRUS (2D/3D)
RCP scenarios
Climate change projections
Drainage flux
Nitrate loss

ABSTRACT

The impact of global warming on water and nitrate losses from a rainfed-canola cropping system under various artificial drainage systems was assessed using an integrated field-modeling approach. Four subsurface drainage systems with different drain depths (D_x) and spacings (L_y), including $D_{0.90}L_{30}$, $D_{0.65}L_{30}$, $D_{0.65}L_{15}$, and Bilevel (with a drain spacing of 15 m and alternate drain depths of 0.65 and 0.90 m), were considered. The HYDRUS (2D/3D) model was first calibrated and validated using data collected for all drainage systems during the 2015–2016 and 2016–2017 canola cropping cycles, respectively, and then applied to simulate water/nitrate losses for different drainage systems under meteorological conditions predicted assuming expected future global warming. Future weather data were downscaled from 20 general circulation models and four RCP scenarios for the mid 21st century (for 2041–2070). The model capability of representing experimental field data was evaluated using the mean bias error (*MBE*), the normalized root mean square error (*nRMSE*), and the model efficiency (*EF*). The HYDRUS (2D/3D) model provided reliable description of soil water contents (*MBE* = -0.5 % to 0.2 %, *nRMSE* = 0.005 − 0.034%, and *EF* = 0.73 − 0.99), drainage fluxes (*MBE* = -21.7 × 10^{-3} to 24.9 × 10^{-3} mm d^{-1}, *nRMSE* = 0.23 − 0.37%, and *EF* = 0.69 − 0.85), soil nitrate concentrations (*MBE* = -0.002 to 1.00 mg cm^{-3}, *nRMSE* = 0.08 − 0.18%, and *EF* = 0.51 − 0.88), and nitrate fluxes (*MBE* = -0.97 to 0.72 mg cm^{-1} d^{-1}, *nRMSE* = 0.35 − 0.57%, and *EF* = 0.77 − 0.87). The modeling results indicate that climate change will cause an increase of up to 148 % in average daily drainage fluxes and up to 125 % in average daily nitrate fluxes compared to the base case. This will result in an increase of 4–125 % in seasonal nitrate losses from various drainage systems, with the lowest and highest projections for the $D_{0.65}L_{15}$ and $D_{0.65}L_{30}$ systems, respectively. The HYDRUS-simulated results indicate that the $D_{0.65}L_{15}$ system is environmentally safer than the other evaluated drainage systems for predicted global warming conditions concerning water/nitrate losses.

1. Introduction

The need to feed the growing global population on the one hand, and increasing global scarcity of blue (fresh) water (WWAP, 2009; Hoekstra et al., 2012) on the other hand, indicate that it is essential to expand rainfed agriculture in the world. In this regard, humid regions may be of higher importance since they receive a sufficient quantity of precipitation to fully supply crop's water requirements by green (from rainfall) water (Shahsavari et al., 2019). However, expanding dry-land farming in these regions may be restricted by waterlogging problems, which occasionally occur after heavy rainfalls and, particularly, in heavy soils (Darzi-Naftchali et al., 2017). Waterlogging threatens the year-round cropping, resulting in considerable areas either going out of production or experiencing reduced yields (Darzi-Naftchali et al., 2013). Under such circumstances, installing subsurface drainage systems may help in providing suitable conditions for winter-crops-based cropping systems and consequently improving the annual productivity of these lands. Subsurface drainage systems can speed up the water table drawdown and provide better aeration during the growing season.

While being beneficial in terms of the water table control, installed drainage systems may cause serious environmental challenges due to their negative impacts on nutrient leaching. Previous researchers have demonstrated that drainage systems may accelerate the leaching process of soil nutrients, and in particular of nitrogen (N) (Kalita et al., 2006; Furukawa et al., 2008; Zhang et al., 2007; Darzi-Naftchali et al., 2017), which is well known to be an essential crop nutrient affecting

* Corresponding author.
E-mail addresses: f.karandish@uoz.ac.ir, f.karandish@utwente.nl, Karandish_h@yahoo.com (F. Karandish).

https://doi.org/10.1016/j.agwat.2020.106420
Received 12 January 2020; Received in revised form 26 July 2020; Accepted 27 July 2020
Available online 31 July 2020
0378-3774/

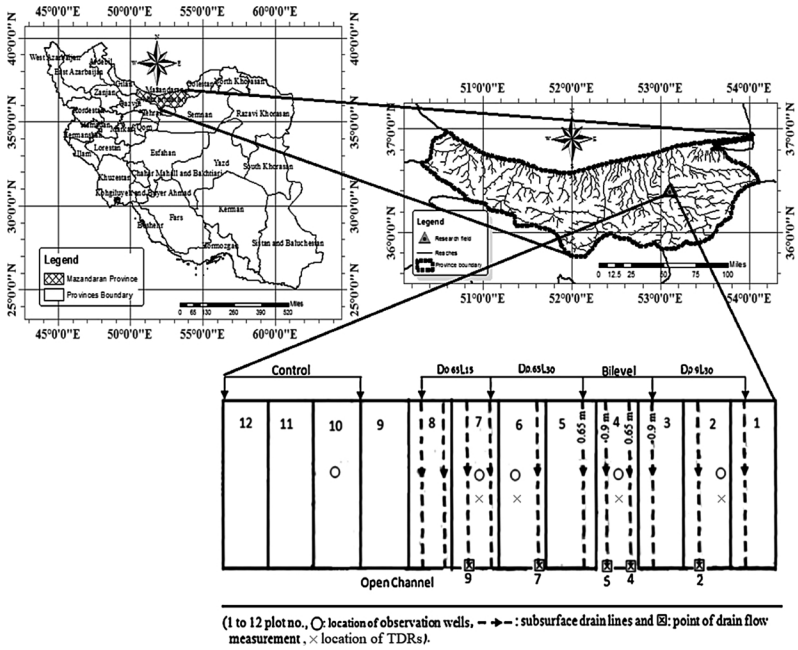

Fig. 1. The location of the study area in Iran (top-left) in the Mazandaran province (top-right), and the schematic of the drainage systems (bottom) (After Darzi-Naftchali et al., 2018).

crop growth and yield (Wienhold et al., 1995; Jia et al., 2014). The design parameters of drainage systems, including the type of the systems and the drain depth and spacing, may affect water or N losses from agricultural lands (Christen and Skehan, 2001; Wahba and Christen, 2006; Jafari-Talukolaee et al., 2015, 2016; Darzi-Naftchali et al., 2017). For certain drainage systems, the rate of water and N losses additionally also depends on field management practices. Improving field management practices may increase the water/nutrient holding capacity of the soil and thus reduce water and N losses (Azooz and Arshad, 1996; De Vita et al., 2007; Triplett and Dick, 2008; Udayasoorian et al., 2009; Constantin et al., 2010; Mitchell et al., 2012; Liu et al., 2013; Phogat et al., 2013; Chukalla et al., 2017).

Drainage fluxes represent a dominant factor for water and N losses from drained areas. Among various influencing factors, climatic variables, including precipitation (P) and potential evapotranspiration (ET_0), play key roles in determining the rate of drainage fluxes. Increased surplus precipitation, defined as P- ET_c, may accelerate the rate of water and N losses due to enhanced drainage fluxes. Water and N losses from drained dry-farming lands may become a more important concern in the future when predicted global warming, which affects these climatic variables, takes place. Numerous researchers have demonstrated various ranges of both negative as well as positive projections of climate change into P and ET_0 in different parts of the world (Abbaspour et al., 2009; Dastoorani and Poormohammadi, 2012; Terink et al., 2013; Agarwal et al., 2014; Kazemi-Rad and Mohammadi, 2015; Karandish et al., 2017; Karandish and Mousavi, 2018; Adham et al., 2019; Darzi-Naftchali and Karandish, 2019). Through such investigations, earlier research has mainly focused on determining probable economic consequences of global warming on the agricultural sector due to the climate change impact on crop yields and productivity under different future greenhouse gas emission scenarios (Karandish et al., 2016; Harmsen et al., 2009; Massah Bavani and Morid, 2005).

Predicting probable N losses under climate change conditions is essential because the byproduct of these losses is the pollution of water resources (Karandish and Šimůnek, 2017) due to N leaching/drainage from agricultural lands (Zhu et al., 2005; Thompson et al., 2007; Dudley et al., 2008; Burow et al., 2010; Dahan et al., 2014; Karandish et al., 2016; Darzi-Naftchali et al., 2017). This issue has higher importance in humid regions, where a low recovery of N fertilizers by crops produces excessive N losses after heavy rains (Karandish and Šimůnek, 2017). Although a few attempts have been made to investigate the effects of climate change on water and N losses in agricultural systems (e.g., Singh et al., 2009; Wang et al., 2015; He et al., 2018; Jiang et al., 2020), a literature review reveals that no such study has been carried out for subsurface-drained paddy fields under winter-rainfed cropping. As such systems are in their infancy in northern Iran paddy fields, a comprehensive study of their behavior would enable policymakers to incorporate the effects of inherent complexities of climate change on drainage activities to protect the local environment.

Therefore, we carried out a field experiment to investigate water and N losses from a drained field cultivated with rainfed-canola and with various subsurface drainage systems. Our research is novel since it is the first study in which environmental hazards in rainfed agriculture due to global warming are evaluated in terms of N losses from the field. To the best of our knowledge, our study assesses for the first time such hazards in fields with subsurface drainage systems. The N dynamics under various climate change projections were assessed using the HYDRUS (2D/3D) model (from now on referred to simply as HYDRUS), which was first calibrated and validated using the field-collected data. We used the HYDRUS model since its capability in capturing drainage and N fluxes has been previously confirmed by many researchers (e.g., Öztekin, 2002; Mirjat et al., 2014; Filipovic et al., 2014; Li et al., 2014; Mguidiche et al., 2015; Karandish and Šimůnek, 2016; Mekala and Nambi, 2016; Darzi-Naftchali et al., 2018; Matteau et al., 2019). The main objectives of this research thus were (i) to calibrate and validate HYDRUS using experimental drainage and nitrate fluxes collected in a subsurface-drained field cultivated with rainfed canola, and (ii) to investigate the impact of climate change projections on key climatic variables, drainage, and nitrate fluxes.

2. Materials and methods

2.1. Field trial

2.1.1. Study area and drainage system layout

The field research was carried out during two canola growing seasons (2015−16 and 2016−17) in the subsurface drainage pilot of the Sari Agricultural Sciences and Natural Resources University in the

Mazandaran province, Iran (SANRU: 36.3∘ N, 53.04∘ E; 15 m below sea level) (Fig. 1). In 2011, this pilot was designed and implemented in a 4.5-ha consolidated paddy field (Darzi-Naftchali et al., 2013, 2018; Darzi-Naftchali and Ritzema, 2018), consisting of four subsurface drainage systems with different drain depths (D_x) and spacings (L_y), including $D_{0.90}L_{30}$, $D_{0.65}L_{30}$, $D_{0.65}L_{15}$, and Bilevel which has a drain spacing of 15 m and alternate drain depths of 0.65 and 0.9 m (Fig. 1). The field consisted of consolidated paddy plots 100 m long and 30 m wide. Considering the dimensions of the plots and the field size, the drainage systems were installed at a scale much larger than the laboratory scale. Drainage installation costs at such a scale were very high and required a large area. Different drainage systems were not replicated due to limited resources and land. The drainage pipes were installed so that the last drain line in each system acted as the first drain line in the adjacent system. Accordingly, at least three drain lines were considered in each drainage system. In addition, the monitoring lines (lines 2, 4, 5, 7, and 9 in Fig. 1) for measuring drain discharge and water quality were selected to fully represent each drainage system by removing the buffering lines. A detailed description of the drainage systems can be found in Darzi-Naftchali et al. (2013, 2018).

Long term averages of annual precipitation, mean temperature, as well as minimum and maximum temperatures recorded in the study area, are 616 mm and 17.3 °C, −6 °C, and 38.9 °C, respectively (Darzi-Naftchali et al., 2018). The variation of climatic variables during the 2015–2016 (the calibration period) and 2016–2017 (the validation period) growing seasons is shown in Fig. 2.

2.1.2. Cropping system and data collection

The area was under rice-canola cropping during 2011–2017, with rice as a major crop and canola as a winter crop. The data from the 2015−16 and 2016−17 canola growing seasons were used in the present study. Canola was cultivated in the two cropping cycles on October 3 in 2015 and on September 28 in 2016. Crops were harvested on May 4, 2016, and May 20, 2017. All agricultural practices were the same as the conventional practices of local farmers in the study area. In the growing season of 2015–2016, 50 kg ha^{-1} of triple superphosphate was applied before cultivation, and 50 kg ha^{-1} of urea (i.e., $CO(NH_2)_2$ with 46 % N) was applied 52 days after sowing (DAS). In the second growing season, urea was applied at rates of 85 kg ha^{-1}, 85 kg ha^{-1}, and 115 kg ha^{-1} at 24, 96, and 116 DASs, respectively. The growers in the region adjust fertilization based on their activities in the crop rotation. For example, remaining residues after the previous crop are considered by the experienced growers (Darzi-Naftchali et al., 2017).

Before crop cultivation, soil samples were collected every 30 cm to a depth of 200 cm to determine soil physical and hydraulic properties and the soil N-content. Soil water characteristic curves of the soil samples were determined by measuring soil water contents at 14 different pressure heads (varied in the range of 0–15 bars). After that, the RETC model was applied to fit the van Genuchten-Mualem model (van Genuchten, 1980) to the observed retention data.

For each treatment, two suction samplers were buried at depths of 30 cm and 60 cm beneath the surface before crop cultivation and remained continuously at 30 kPa. The samplers had porous ceramic caps of 5 cm in diameter. Using the vacuum pump, the leachate was then collected during the growing seasons (once every two weeks). Nitrate concentrations of water samples were determined by spectrophotometer (DR-4000 HACH).

To determine daily variations in the soil water content (SWC) during the cropping cycles, a 100-cm long TDR probe (Trime FM; IMKO; Germany) was installed midway between drains in each subsurface drainage system (i.e., 4 TDR probes were installed in the study area; 1 probe * 4 drainage systems). TDR probes were used once a day to measure SWC at a 15-cm interval during both growing seasons. The accuracy of all TDR sensors was evaluated by comparing TDR-measured SWCs with corresponding values measured using the gravimetric method. TDR-measured SWCs agreed well with gravimetrically-measured SWCs with a coefficient of determination of 95 %.

Water table depths were measured daily in observation wells that were dug out midway between adjacent drains in each drainage system. Free drainage management was adopted during canola growing seasons. Subsurface drainage discharges (q) were measured daily for all drainage systems as long as the flow was observed at the outlet of drains. Drain fluxes were measured by using partial flumes at the outlet of representative drains during drainage periods. The total water discharge for a particular day is the sum of discharges over 24 h. The above values were converted to water depths by dividing them with the plot area. Drainage water samples were taken every 15 days and several consecutive days after fertilization. Collected water samples were then analyzed to determine their nitrate concentrations.

2.2. Climate data under global warning

The projections of future climate data were downscaled for four RCP scenarios (the Representative Concentration Pathways reported in the 5th IPCC report, IPCC, 2013): the RCP2.6 (a low greenhouse gases emission scenario), RCP4.5 (an intermediate one), RCP6.5 (a high one), and RCP8.5 (a very high greenhouse gases emission scenario). For each scenario, the projections of air temperature (minimum and maximum),

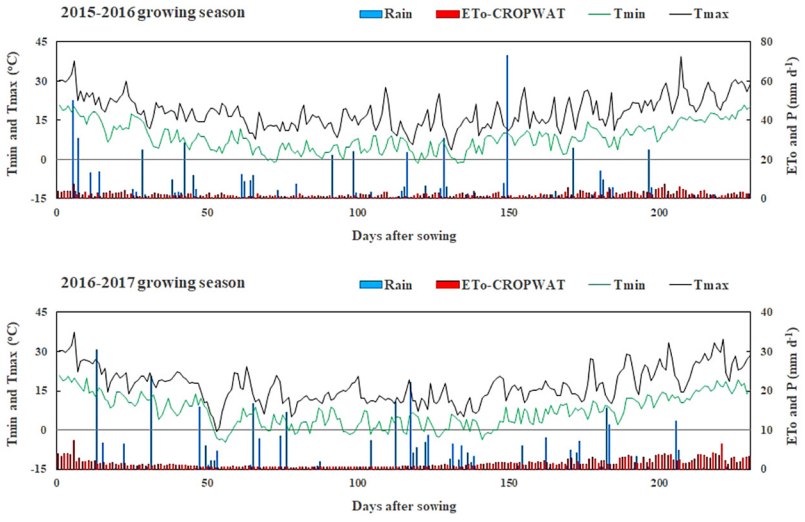

Fig. 2. Climatic variables in the study area during the 2015-2016 (the calibration period) and 2016-2017 (the validation period) growing seasons.

Table 1
Selected GCMs (Global Climate Models) for the current study.
(Source: Miao et al. (2014).

Model	Source
ACCESS 1.0	Common Wealth Scientific and Industrial Research Organization and Bureau of Meteorology, Australia
BCC-CSM1.1	Beijing Climate Center, China Meteorological Administration, China
BNU-ESM	Beijing Normal University, China
CanESM	Canadian Center for climate modeling and analysis, Canada
CCSM4	National Center for Atmospheric Research (NCAR), USA
CESM1.0-BGC	National Center for Atmospheric Research (NCAR), USA
CISRO-MK3	Australian Common Wealth Scientific and Industrial Research Organization
GFDL-ESM2G	Geophysical Fluid Dynamic Laboratory, USA
GFDL-ESM2M	Geophysical Fluid Dynamic Laboratory, USA
HadGEM2-CC	Met office Hadley Center, UK
HadGEM2-ES	Met office Hadley Center, UK
inmcm4	Institute of Numerical Mathematics, Russian Academy of Sciences
IPSL-CL5A-LR	Institute Pierre-Simon Laplace, France
IPSL-CL5A-MR	Institute Pierre-Simon Laplace, France
MIROC	Japan Agency for Marin-Earth Science and Technology, Atmosphere and Ocean Research Institute (University of Tokyo Japan)
MIROC-ESM	Japan Agency for Marin-Earth Science and Technology, Atmosphere and Ocean Research Institute (University of Tokyo Japan)
MPI-ESM-LR	Max Plank Institute for Meteorology (MPI-M), Germany
MPI-ESM-MR	Max Plank Institute for Meteorology (MPI-M), Germany
MRI-CGCM3	Meteorological Research Institute of Japan
Nor-ESM1-M	Norwegian Climate Center, Norway

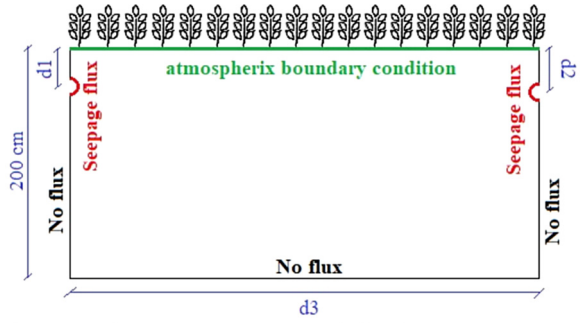

Fig. 3. The transport domain and boundary conditions considered in the HYDRUS model for simulating water flow and solute transport.

precipitation, solar net radiation, wind speed, atmosphere pressure, and relative humidity were generated using 20 different GCM models (general circulation models, Table 1) for the future period of 2040–2070, and compared with the corresponding values obtained for the base period (1975–2005).

The statistical downscaling approach was carried out based on the widely used change factor method (Jones et al., 1997). For all climatic variables, the change factor coefficients, which determine the relationship between the current and future climatic variables, were calculated based on Eq. 1 (Jones et al., 1997), except for air temperature, for which Eq. 2 was applied (Trzaska and Schnarr, 2014).

$$\Delta P_i = \left(\frac{\overline{P}_{GCM,\,fut,\,i}}{\overline{P}_{GCM,\,base,\,i}}\right) \quad (1)$$

$$\Delta T_i = \left(\overline{T}_{GCM,\,fut,\,i} - \overline{T}_{GCM,\,base,\,i}\right) \quad (2)$$

wheres ΔP_i is a dimensionless monthly change factor for a particular climatic variable (p), $\overline{P}_{GCM,\,fut,\,i}$ and $\overline{P}_{GCM,\,base,\,i}$ are monthly averages of future (simulated) and historical values of a considered climatic variable, respectively, ΔT_i is a dimensionless monthly change factor for air temperature, and $\overline{T}_{GCM,\,fut,\,i}$ and $\overline{T}_{GCM,\,base,\,i}$ are monthly averages of future and historical values of air temperature, respectively. These change factors were calculated at a monthly time scale (i = 1–12).

Using generated climatic variables, reference evapotranspiration (ET_0) was calculated using the Penman-Monteith FAO-56 equation (PMF) (Allen et al., 1998) due to its global acceptability (Karandish et al., 2017). ET_0 was then used to estimate crop evapotranspiration as explained below.

2.3. N dynamics under current and future conditions

2.3.1. The HYDRUS model

2.3.1.1. Model description and governing equations. Soil water and N dynamics were simulated using the HYDRUS (2D/3D) model (Šimůnek et al., 2008, 2016). The HYDRUS program numerically solves the Richards equation for saturated-unsaturated water flow:

$$\frac{\partial \Theta(h)}{\partial t} = \frac{\partial}{\partial x}\left(K(h)\frac{\partial h}{\partial x}\right) + \frac{\partial}{\partial z}\left(K(h)\frac{\partial h}{\partial z}\right) - \frac{\partial K(h)}{\partial z} - WU(h, x, z) \quad (3)$$

where Θ is the volumetric soil water content (SWC) [L^3L^{-3}], K is the unsaturated hydraulic conductivity [LT^{-1}], h is the soil water pressure head [L], x is the lateral coordinate [L], z is the vertical coordinate

Table 2
Soil properties, and soil hydraulic and solute transport parameters for the study area (i.e., the calibrated and validated data for soil water and solute transports are obtained through HYDRUS modeling).

Soil depth (cm)	OM (%)	Clay (%)	Silt (%)	Sand (%)	θ_r	θ_s	α	n	l	K_s (cm d^{-1})	D_L	D_T
0 – 30		48.5	44.4	7	0.001	0.40	0.004	1.193	0.5	25.6	35.4	3.7
30 – 60		55.5	42	2.5	0.001	0.40	0.008	1.119	0.5	8.1	30.6	3.4
60 – 90		46.5	45.5	8	0.192	0.40	0.008	1.355	0.5	20.7	22.5	2.5
90 – 120		42.5	51.5	6	0.098	0.40	0.006	1.423	0.5	16.3	16.1	2.0
120 – 150		52	42	6	0.001	0.57	0.004	1.274	0.5	10.9	13.2	1.3
150 – 200		58.5	35.5	6	0.229	0.59	0.004	1.467	0.5	8.3	7.2	0.6

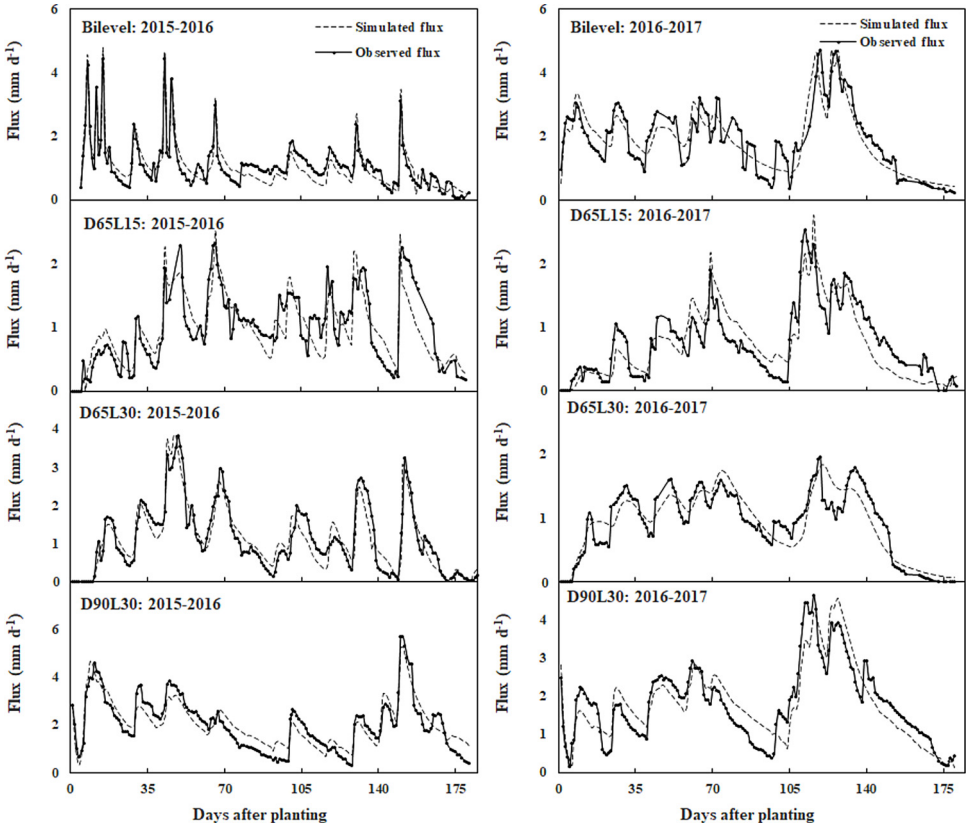

Fig. 4. Observed and simulated drainage fluxes during the 2015-2016 (left, calibration) and 2016-2017 (right, validation) growing seasons for different drainage systems (Bilevel, $D_{0.65}L_{15}$, $D_{0.65}L_{30}$, and $D_{0.90}L_{30}$).

(positive downwards), t is time [T], and $WU(h, x, z)$ is root water uptake [T^{-1}], which is calculated as follows:

$$WU(h, x, z) = \gamma(h) RDF(x, z) WT_{pot} \tag{4}$$

where $\gamma(h)$ is the soil water stress response function (dimensionless) of Feddes et al. (1978), *RDF* is the normalized spatial root water uptake distribution [L^{-2}], T_{pot} is the potential transpiration rate [LT^{-1}], and W is the width of the soil surface [L] associated with the transpiration process. The stress response function was obtained from the HYDRUS database for maize (Šimůnek et al., 2011). Uniform root distribution was assumed in each soil layer. The van Genuchten-Mualem constitutive relationships were used to model soil hydraulic properties (van Genuchten, 1980).

The transport of nitrate (NO_3^-) was modeled using the convection-dispersion equation embedded in the HYDRUS model. This equation is reported to be suitable for conservative solutes such as NO_3^-:

$$\frac{\partial \theta c}{\partial t} = \left\{ \frac{\partial}{\partial x}\left(\theta D_{xx} \frac{\partial c}{\partial x} + \theta D_{xz} \frac{\partial c}{\partial z} \right) + \frac{\partial}{\partial z}\left(\theta D_{zz} \frac{\partial c}{\partial z} + \theta D_{zx} \frac{\partial c}{\partial x} \right) \right\} - \left(\frac{\partial q_x c}{\partial x} + \frac{\partial q_z c}{\partial z} \right) - S_c \tag{5}$$

where c is the NO_3^- concentration in the liquid phase (ML^{-3}), q_x and q_z are the components of the volumetric flux density (LT^{-1}), D_{xx}, D_{zz}, and D_{xz} are the components of the dispersion tensor (L^2T^{-1}) (Bear, 1972), S_c is a sink term, which generally includes local NO_3^- uptake (through a passive process), mineralization, microbial immobilization, and denitrification ($ML^{-3}T^{-1}$). The first term on the right side of Eq. 3 describes the solute flux due to dispersion, the second term describes the solute flux due to convection with flowing water, and the third term describes nutrient uptake by roots.

Similarly, as in other earlier studies (e.g., Ajdary et al., 2007; Wang et al., 2010; Tafteh and Sepaskhah, 2012), mineralization gains were neglected due to the following reasons. First, the lack of organic matter (OM) lmits the mineralization process in mineral soils (i.e., soils with OM < 3% in the upper horizon, Huang et al., 2009 cronologically.), as in our study, the lack of OM limits the mineralization process (Li et al., 2003; Deenik, 2006; Wijanarko, 2015). Second, mineralization mainly occurs in coarse-textured soils with low clay content, while it decreases considerably as soil clay content increases (Karandish and Šimůnek, 2017). Third, the abundance of micropores in high clay soils causes a physical protection of OMs from being microbially decomposed and mineralized (Deenik, 2006). Our frequent measurements also showed that NO_3^- concentration in the soil were much higher than NH_4 concentrations (Darzi-Naftchali et al., 2016). Only the NO_3^- transport in the soil was thus considered in this research, assuming that the input of N-fertilizer in the form of urea was instantly nitrified into NO_3-. This is similar to the assumptions made by many other researchers (e.g., Ajdary et al., 2007; Tafteh and Sepaskhah, 2012; Karandish and Šimůnek, 2017), who assumed that nitrification is faster than the other processes, and nitrifying urea into NO_3-takes only a few days (Havlin et al., 2006). In addition, nitrification is reported to be stimulated in less-organic (OM < 3%), finely-textured soils with high clay content, all of which are the cases in the current research.

We also considered that root N uptake was strictly passive, which has also been assumed in many other studies (e.g., Hanson et al., 2006; Tafteh and Sepaskhah, 2012). According to this assumption, N uptake can be calculated by multiplying the local soil N concentration and root water uptake.

2.3.1.2. Flow domain, and initial and boundary conditions. The impermeable layer in the study area was located at a soil depth of 200 cm (Fig. 3). Hence, the 2D transport domain was defined as a rectangle with a depth of 200 cm and a width of 30 m for $D_{0.9}L_{30}$ and $D_{0.65}L_{30}$ drainage systems and 15 m for the $D_{0.65}L_{15}$ and Bi-level

Table 3
Model performance criteria for different drainage systems during calibration (2014-2015) and validation (2016-2017). MBE, nRMSE, and EF are the mean bias error, the normalized root mean square error, and the model efficiency coefficient, respectively.

Parameter	Treatment	Soil depth (cm)	Calibration period			Validation period		
			MBE[a]	nRMSE (nd[b])	EF (%)	MBE[a]	nRMSE (nd[b])	EF (%)
Solute Flux	Bilevel	–	0.463	0.415	0.795	0.718	0.570	0.806
	$D_{0.65}L_{15}$	–	0.630	0.418	0.870	−0.008	0.498	0.772
	$D_{0.65}L_{30}$	–	0.568	0.386	0.841	0.354	0.395	0.846
	$D_{0.90}L_{30}$	–	−0.266	0.353	0.772	−0.972	0.436	0.769
Solute concentration	Bilevel	0 − 30	0.001	0.097	0.883	−0.001	0.091	0.842
		30 − 60	0.001	0.100	0.863	0.001	0.120	0.868
	$D_{0.65}L_{15}$	0 − 30	−0.002	0.112	0.839	0.001	0.079	0.844
		30 − 60	0.001	0.080	0.868	0.001	0.184	0.513
	$D_{0.65}L_{30}$	0 − 30	−0.001	0.106	0.850	−0.001	0.136	0.808
		30 − 60	0.001	0.079	0.843	−0.001	0.132	0.778
	$D_{0.90}L_{30}$	0 − 30	0.001	0.152	0.829	0.001	0.169	0.833
		30 − 60	0.001	0.114	0.883	−0.001	0.128	0.798
Drainage flux (q)	Bilevel	–	−0.26	0.286	0.822	24.9	0.251	0.787
	$D_{0.65}L_{15}$	–	−1.51	0.311	0.688	−1.11	0.370	0.719
	$D_{0.65}L_{30}$	–	2.37	0.291	0.850	−1.96	0.247	0.716
	$D_{0.90}L_{30}$	–	−21.7	0.230	0.822	0.39	0.259	0.778
Soil water content	Bilevel	0 − 30	0.002	0.025	0.840	−0.001	0.034	0.851
		30 − 60	−0.001	0.022	0.946	0.001	0.029	0.945
		60 − 90	0.000	0.015	0.986	−0.005	0.033	0.959
	$D_{0.65}L_{15}$	0 − 30	−0.002	0.024	−0.016	−0.001	0.014	0.745
		30 − 60	0.001	0.022	0.864	0.001	0.018	0.916
		60 − 90	0.000	0.016	0.864	−0.001	0.018	0.872
	$D_{0.65}L_{30}$	0 − 30	−0.001	0.027	0.826	−0.001	0.031	0.848
		30 − 60	0.001	0.029	0.790	−0.001	0.032	0.815
		60 − 90	0.001	0.023	0.967	0.001	0.018	0.962
	$D_{0.90}L_{30}$	0 − 30	0.001	0.005	0.726	0.001	0.006	0.764
		30 − 60	0.001	0.005	0.838	−0.001	0.008	0.772
		60 − 90	0.001	0.006	0.795	−0.001	0.008	0.902

[a] MBE is described in mg cm^{-1} d^{-1} for solute fluxes, in mg cm^{-3} for soil NO_3 concentrations, in 10^{-3} mm d^{-1} for drainage fluxes, and in cm^3 cm^3 for soil water contents.
[b] nd means “no dimension”.

drainage systems. The drains are considered to be on the sides of the transport domain. An unstructured triangular finite element mesh (FEM) was used to discretize the defined transport domain. A non-uniform FEM was generated by HYDRUS with finite element sizes gradually increasing with distance from the drains. The entire transport domain was divided into six soil layers, i.e., 0 − 30 cm, 30 − 60 cm, 60 − 90 cm, 90 − 120 cm, 120 − 150 cm, and 150 − 200 cm soil depths, for which different soil properties were defined. To represent the high permeability of the backfilled drain trench (gravel), an additional soil layer was defined 10 cm around, 10 cm below, and 30 cm above the drains. Measured soil water contents in different soil layers were considered to represent initial conditions for water flow simulations. The saturated soil water content was specified as an initial condition in soil layers below the water table to differentiate the saturated and unsaturated zones.

The atmospheric boundary condition, defined using potential evaporation (E_P), potential transpiration (T_P), and precipitation (P), was applied at the top of the transport domain. The dual-crop coefficient approach (Allen et al., 1998) was adopted to separate crop evapotranspiration (ET_C) into E_P and T_P as follows:

$$\begin{cases} ET_C = Kc \times ET_0 = E_P + T_P \\ E_P = K_e \times ET_0 \\ T_P = K_{cb} \times ET_0 \end{cases} \quad (6)$$

where K_C is the crop coefficient, K_{Cb} is the basal crop coefficient, and K_e is the evaporation coefficient. The values of K_{Cb} for different crowing seasons were taken from Allen et al. (1998): 0.3, 1.05, and 0.25 for the initial, mid-, and late- growing stages of canola, respectively. The values of K_e were then estimated as 0.05, 0.1, and 0.1, for then mentioned growing stages, respectively. A seepage face boundary condition was used to represent the drains. All other remaining boundaries were assigned a no-flow boundary condition.

The initial condition for solute transport simulations was defined using the measured soil NO_3^- content in different soil layers. A third-type Cauchy boundary condition was used to describe the concentration flux at the top boundary and the drains. A Cauchy boundary condition is automatically converted into a second-type Neumann boundary condition during periods of drain outflow.

2.3.1.3. Calibration and validation. The experimental data were first used to calibrate soil hydraulic and solute transport parameters and then to validate the HYDRUS model. These parameters were optimized using the inverse solution option of HYDRUS. In this process, soil hydraulic parameters, including the saturated hydraulic conductivity (K_s), the saturated soil water content (θ_s), the residual soil water content (θ_r), and solute transport parameters, including the longitudinal (D_L, L) and transverse (D_T, L) dispersivities, were optimized. Measured drain fluxes (q) and NO_3^- concentrations in the 2015–2016 growing season were used to calibrate the HYDRUS model. The calibrated parameters were then used to validate the model using the same data collected in the 2016–2017 growing season. The molecular diffusion coefficient was always set equal to zero since molecular diffusion in soils can usually be neglected (Radcliffe and Šimůnek, 2010; Karandish and Šimůnek, 2017).

2.3.1.4. Correspondence criteria indices. The capability of the HYDRUS model to simulate drainage water and nitrate fluxes under different treatments was assessed using the mean bias error (*MBE*), the normalized root mean square error (*nRMSE*), and the model efficiency index (*EF*) as follows (Karandish and Šimůnek, 2016):

$$MBE = \frac{\sum_{i=1}^{n} (O_i - P_i)}{n} \quad (7)$$

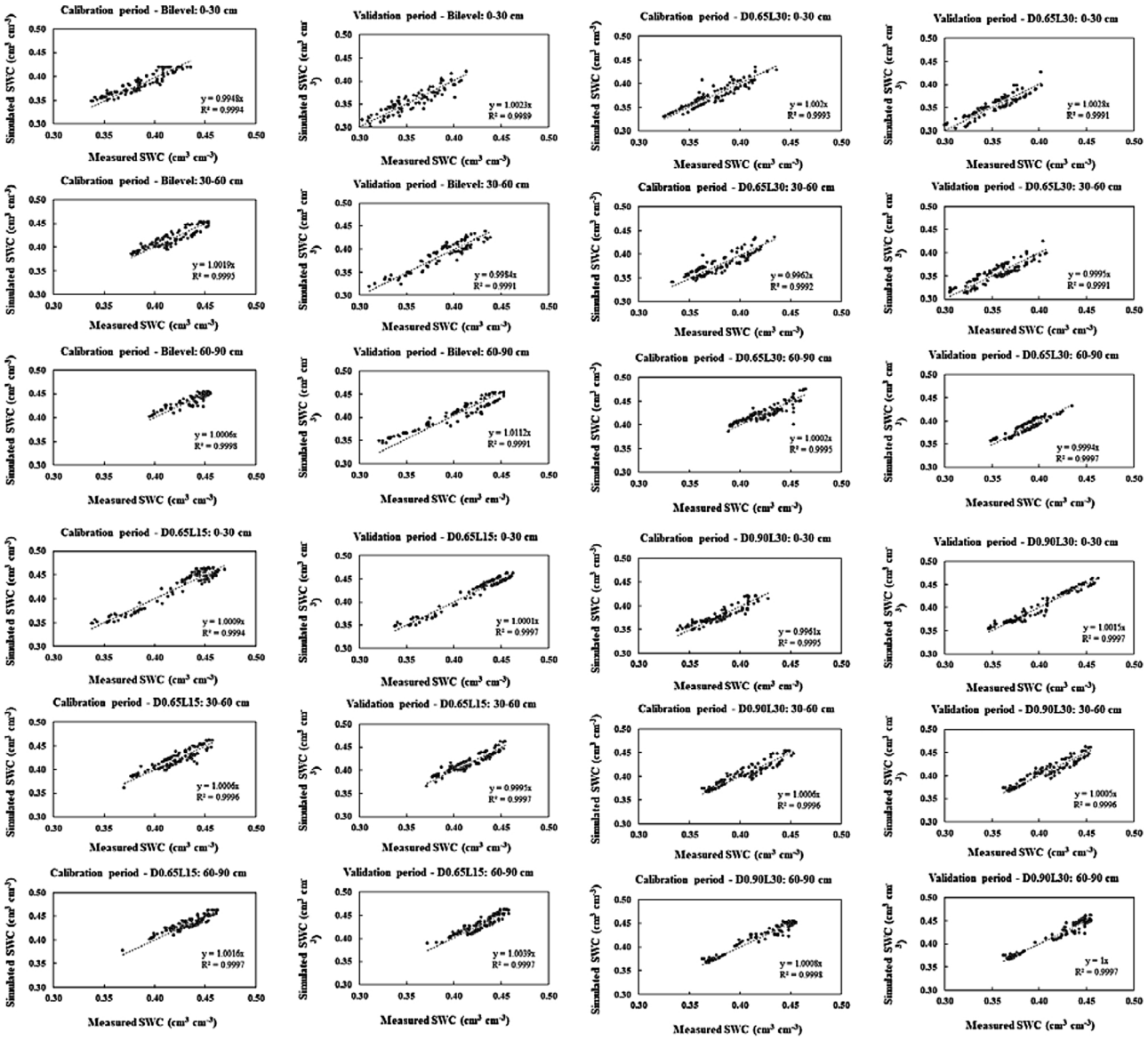

Fig. 5. Scatter plots between the measured and simulated soil water contents (SWC, $cm^3\ cm^{-3}$) at different depths (0-30, 30-60, and 60-90 cm) during the 2015-2016 (calibration; the first and third columns) and 2016-2017 (validation; the second and fourth columns) growing seasons for different drainage systems (Bilevel (top left), $D_{0.65}L_{15}$ (bottom left), $D_{0.65}L_{30}$ (top right), and $D_{0.90}L_{30}$ (bottom right)).

$$nRMSE = \frac{\left\{ {}^{1}/_{n}[\sum_{i=1}^{n}(P_i - O_i)^2]\right\}^{0.5}}{\overline{O}} \tag{8}$$

$$EF = 1 - \frac{\sum_{i=1}^{n}(O_i - P_i)^2}{\sum_{i=1}^{n}(O_i - \overline{O_i})^2} \tag{9}$$

where P_i and O_i are simulated and observed data, respectively, $\overline{O}$ and $\overline{P}$ are the averages of observed and simulated data, respectively, and n is the number of observations.

2.3.2. Scenario analysis

The calibrated and validated HYDRUS model was then applied to estimate the probable consequences of climate change projections on drainage water (q) and NO_3^- fluxes for different drainage systems. The climate projections were first generated for the base period (i.e., 1975–2005), and then for all 20 GCMs for four considered RCP scenarios over the 2040–2070 period. To obtain consistent comparisons, the initial and boundary conditions, as well as all agricultural practices, were considered to be the same as during the validation period (i.e., the 2016–2017 growing season). A comparative analysis was then carried out between the simulated projections for the 2041–2070 period and the base period. In this regard, a relative change in the considered parameter (i.e., climatic variables, drainage flux, NO_3 flux, or seasonal N loss) was calculated as follows:

$$RC = \frac{X_f - X_b}{X_b} \times 100\% \tag{10}$$

where RC is a relative change in the considered parameter (%), X_f and X_b are values of the considered parameter in the future and base periods, respectively.

3. Results and discussion

3.1. The HYDRUS(2D/3D) model efficiency

The calibrated soil hydraulic and solute transport parameters are summarized in Table 2. Fig. 4 shows temporal variations of the observed and HYDRUS-simulated drain fluxes (q) for different drainage

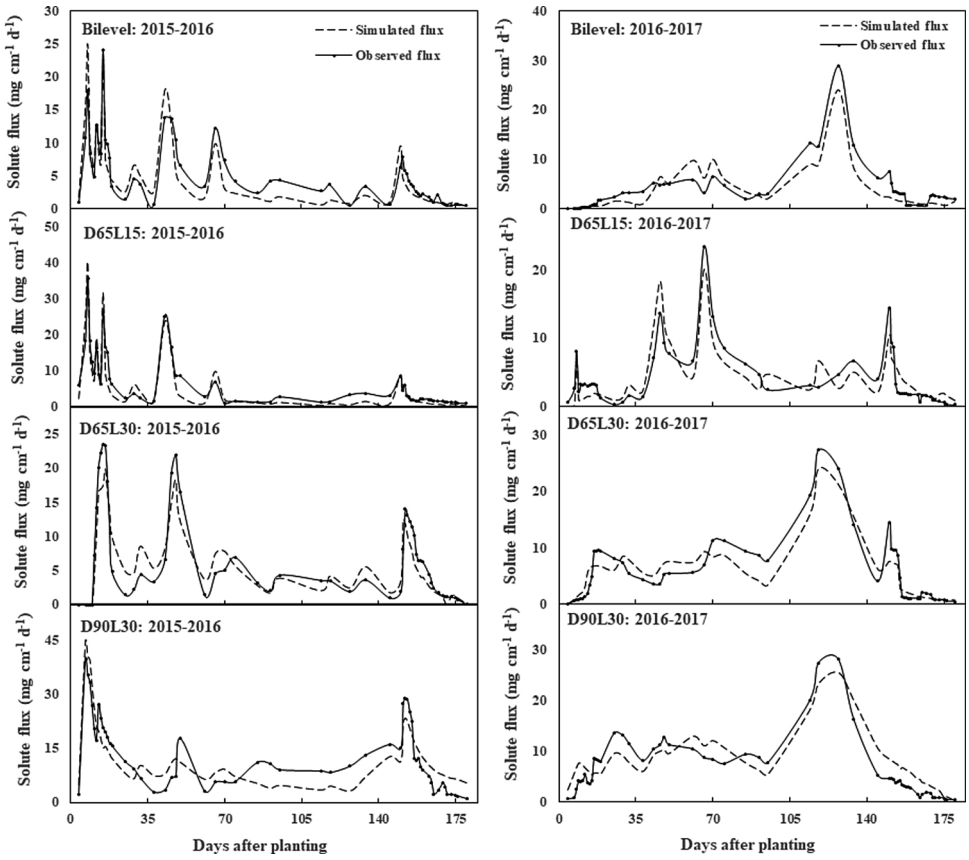

Fig. 6. Observed and simulated NO_3^- fluxes during the 2015-2016 (left charts, the calibration period), and 2016-2017 (right charts, the validation period) growing seasons for different drainage systems (Bilevel, $D_{0.65}L_{15}$, $D_{0.65}L_{30}$, and $D_{0.90}L_{30}$).

systems during the calibration (2015–2016 growing season) and validation (2016–2017) periods. The model captured the temporal pattern of drainage fluxes *q* in both periods for all drainage systems well, even though different drainage systems did not display the same patterns. In the 2015–2016 growing season, the average observed drainage fluxes *q* for the Bilevel, $D_{0.65}L_{15}$, $D_{0.65}L_{30}$, and $D_{0.90}L_{30}$ drainage systems were 1.08, 0.97, 1.13, and 2.05 mm d^{-1}, respectively, while the corresponding HYDRUS-simulated values were 1.07, 0.98, 1.12, and 2.07 mm d^{-1}, respectively. The observed and HYDRUS-simulated values matched even better during the validation period.

The model performance criteria, summarized in Table 3, also indicate the strong predictive capability of the model. *MBE*, *nRMSE,* and *EF* ranged from -21.7 × 10^{-3} to 24.9 × 10^{-3} mm d^{-1}, from 23 % to 37 %, and from 0.69 to 0.85, respectively, among different drainage systems and different growing seasons. The efficiency of the HYDRUS model to predict drainage fluxes *q* is also supported by other researchers (e.g., Öztekin, 2002; Mirjat et al., 2014; Filipovic et al., 2014; Li et al., 2014; Darzi-Naftchali et al., 2018; Matteau et al., 2019).

The quantitative assessment of the model performance, as well as the visual inspection presented in Fig. 5, also shows good agreement between the observed and HYDRUS-simulated soil water contents (SWCs) in different soil layers during the calibration and validation periods; with *MBE*, *nRMSE*, and *EF* ranging from -0.005 to 0.002 cm^3 cm^{-3}, from 5 to -3.4 %, and from 0.73 to 0.99, respectively. These differences may be a consequence of the fact that the HYDRUS-simulated SWCs are compared with the measured SWCs, which are averaged over a certain soil volume, in which the SWC gradient caused by irrigation/precipitation/drainage may not be linear (Karandish and Šimůnek, 2016; Mguidiche et al., 2015). The capability of the HYDRUS model to predict SWC variations is also supported by other researchers (Ramos et al., 2012; Kandelous et al., 2012).

Table 3 also shows good correspondence between the observed and HYDRUS-simulated NO_3 concentrations in different soil layers during both growing seasons (*MBE* = (-0.002)-(+0.001) mg cm^{-1} d^{-1}, *nRMSE* = 7.9–18.4 %, *EF* = 0.51 − 0.88), which indicates that the calibrated model is well suited to describe the flow and transport processes observed in the experimental field.

To ensure the capability of the HYDRUS model to simulate the solute transport adequately, we also compared temporal variations of the observed and simulated NO_3 fluxes in different drainage systems during the calibration and validation periods (Fig. 6). While the HYDRUS model either slightly underpredicted or overpredicted NO_3 fluxes during different periods, the simulated fluxes overall closely matched the observed data for all drainage systems during both the calibration and validation periods, with correlation efficiencies of 0.77 − 0.9 (data not shown). The model performance criteria reported in Table 3 also indicate the high potential of the HYDRUS model in capturing the NO_3 transport in different drainage systems. *MBE*, *nRMSE*, and *EF* varied in the range of (-97)-(0.72) mg cm^{-1} d^{-1}, 35.5–57 %, and 0.77 − 0.87, respectively, across different drainage systems and during both growing seasons. The model capability of simulating N dynamics under different drainage conditions is also supported by others (e.g., Mekala and Nambi, 2016; Matteau et al., 2019).

3.2. Global warming projections

3.2.1. Climatic variables

Fig. 7 shows the range of relative changes in different climatic variables for different RCPs, along with the range of GCMs projections for each scenario. Regardless of the type of the climatic variable, Fig. 7 shows a different behavior of projected variables for different GCMs and RCP scenarios, which could be attributed to different resolutions of

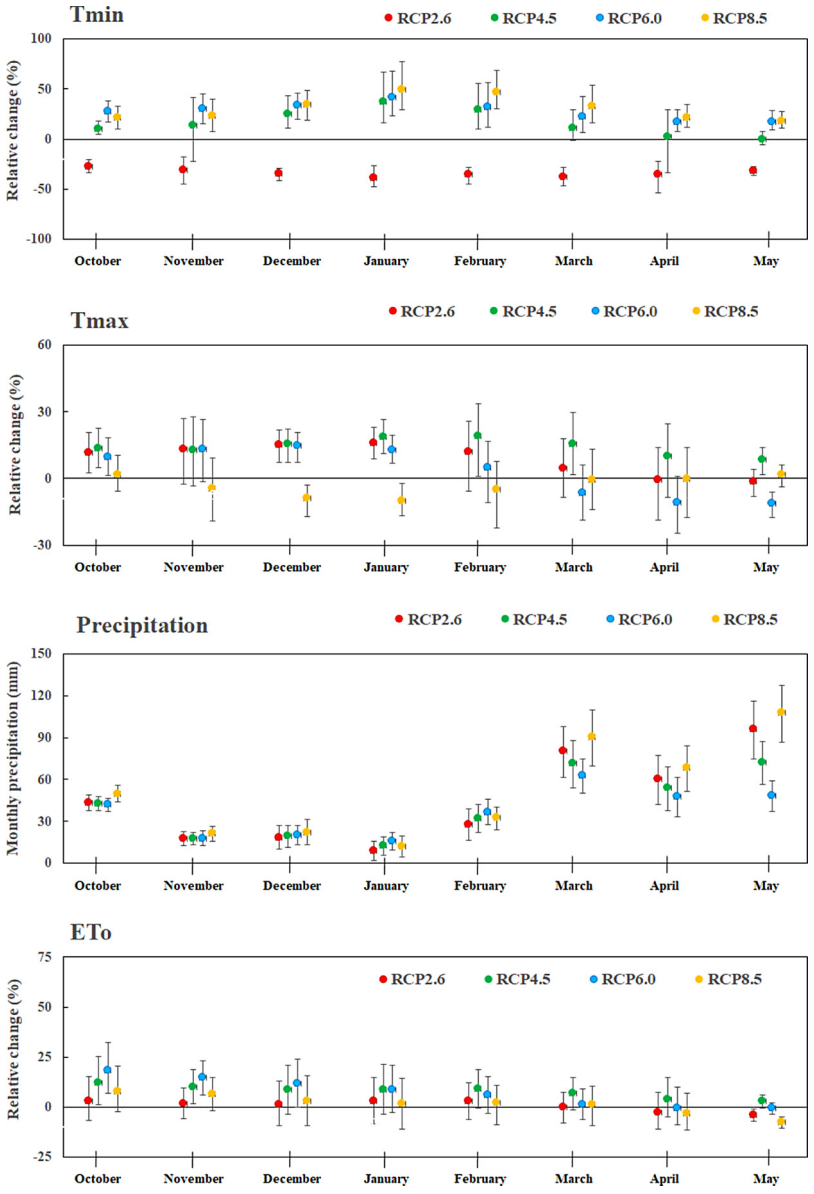

Fig. 7. The range of relative changes in minimum (T_{min}) and maximum (T_{max}) temperatures, monthly precipitation, and monthly ET_0 in the study area for different future RCP scenarios (i.e., 2041-2070) compared to the base period (i.e., 1975-2005). The lower and upper ends indicate the 5% and 95 % intervals of the uncertainty ranges, and dots show the 50 % value.

the ocean models for different GCMs. Climate processes fully depend on how GCMs simulate the extent of sea ice, sea surface temperature, surface heat, ocean heat transfer, and momentum fluxes (CCSP, 2008; Karandish et al., 2017; Karandish and Mousavi, 2018). Different projections by different GCMs could also be attributed to many other factors, which control the simulation process, such as the prognostic variable for cloud characterization and the compatibility between the heat and water budgets of the atmospheric and ocean models (Randall et al., 2007). However, these differences among RCP scenarios can be attributed to the embedded assumptions in the socio-economic and environmental models for each scenario. Other researchers have also indicated that future projections of climate variables depend on either the RCP scenarios or the selected GCM (e.g., Adham et al., 2019; Haj-Amor et al., 2020).

Climate change projections showed both positive (increases) and negative (decreases) changes in monthly average values of T_{max} and ET_0, while monthly precipitation P is more likely to increase in the future. Except for RCP2.6 and a few GCMs for RCP4.5, climate change may cause an increase in T_{min} in the study area. Differences among the projections of different GCMs/RCP scenarios indicate the uncertainty in the projections of future climatic variables. Quantifying these ranges of uncertainties is essential since they provide more accurate insights for developing rational plans to cope with plausible consequences of global warming. Fig. 7 shows that the range of uncertainty arising from projections of different GCMs for different RCP scenarios is lower for T_{min} and T_{max}, which indicates more similar predictions of temperatures compared to water fluxes, such as P and ET_0. Such results are in agreement with those reported by Karandish et al. (2017).

Fig. 7 also demonstrates non-uniform temporal projections of climatic variables by different RCP scenarios, which is also confirmed by others (e.g., Zickfeld et al., 2005; Girvetz et al., 2009; Harmsen et al., 2009; Agarwal et al., 2014; Adham et al., 2019). Precipitation projections seem to be less uncertain over the October-January period, while smaller uncertainties in the projections of other variables were observed in May.

Fig. 7 shows that compared to the base period, and based on the average value obtained from all GCMs under four RCPs, T_{min} may increase by 0.15–1.25 °C, with the lowest and highest increases in April

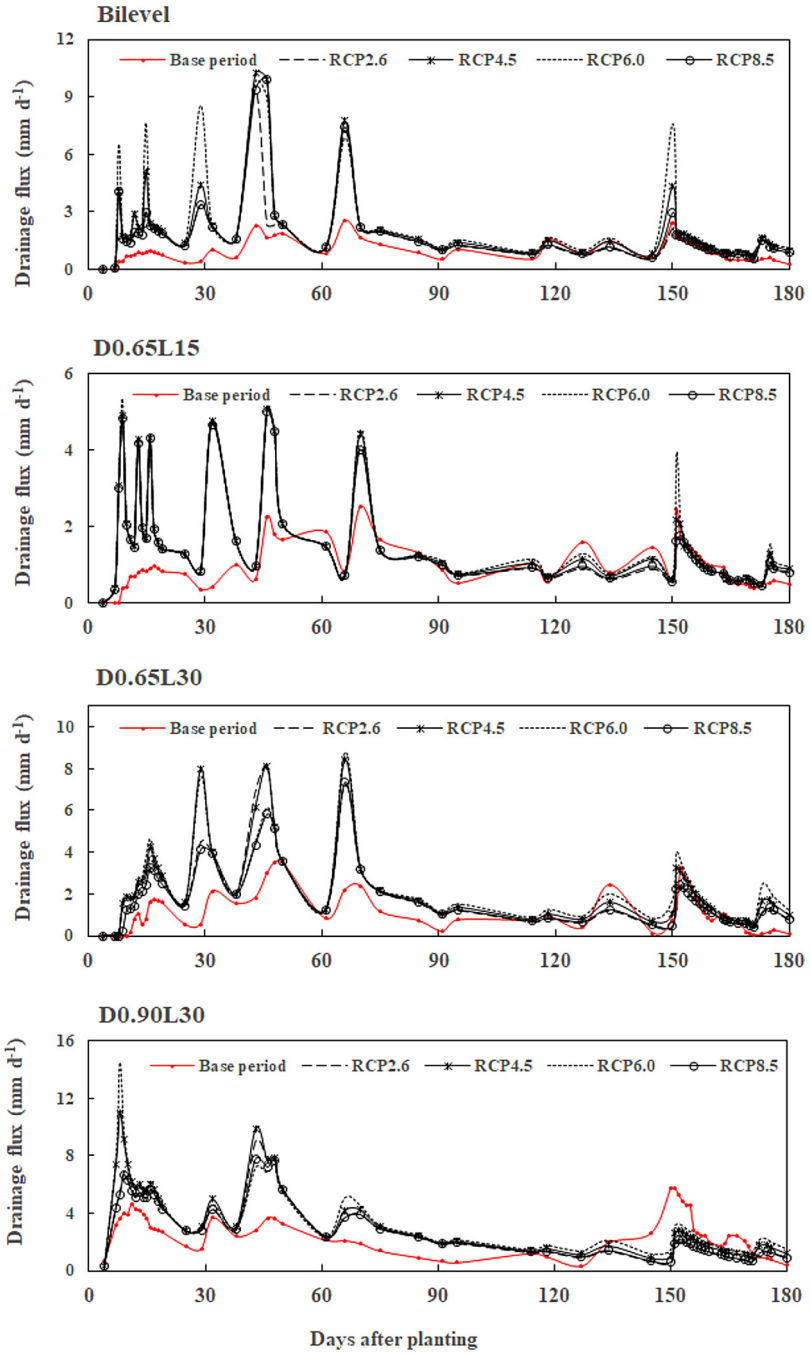

Fig. 8. Temporal variations of drainage fluxes for different drainage systems (Bilevel, $D_{0.65}L_{15}$, $D_{0.65}L_{30}$, and $D_{0.90}L_{30}$) for the base period (1975-2005) and the 2041-2070 period for different RCPs (data are provided based on the ensemble average of 20 GCMs for each RCP scenario).

and October, respectively. T_{max} may increase by 0.45–2.18 °C, except in April and May, when T_{max} decreases by 0.08 °C and 0.15 °C, respectively. Others have reported a general increase in both T_{min} and T_{max} under climate change in the study area (e.g., Abbaspour et al., 2009; Dastoorani and Poormohammadi, 2012; Kazemi-Rad and Mohammadi, 2015; Karandish et al., 2017). They also indicated a non-uniform pattern of temporal projections of global warming into air temperature, which is in agreement with results in our research. An increase in T_{min} in autumn and winter may be beneficial since it may provide favorable conditions for early cultivation and, consequently, may reduce the duration of the cropping cycle since the crop's thermal energy requirement may be supplied during a shorter period (Karandish et al., 2016). Such projections may further lead to lower crop water requirements if the positive effect of the shortened cropping cycle goes beyond the other probable negative effects of global warming on crop growth.

During the 2041–2070 period, monthly P in the study area will always increase with the lowest increase occurring over the November-January period, and the highest one over the March-May period (Fig. 7). The RCP8.5 scenario led to the highest increases in monthly precipitation. Karandish et al. (2016) carried out a high-resolution assessment for entire Iran and reported that global warming might cause the highest increase in P along the coast of the Caspian sea, where the study area is located. They believed that such an increase might be attributed to an increase in air temperature, which consequently causes a considerable increase in the atmospheric water-holding capacity. An increase in P during wet seasons, which is in agreement with the findings of other researchers (e.g., Agarwal et al., 2014; Adham et al., 2019), may cause water-logging challenges, indicating the necessity of

Table 4
Climate change effects on average drainage fluxes (q), average NO_3 fluxes, and seasonal NO_3 losses under different drainage systems during the growing season (ensemble averages for 20 GCMs for each scenario; the base period refers to the 1975-2005 period).

Treatment	Scenario	Drain flux (mm d^{-1})	Nitrate flux (mg cm^{-1} d^{-1})	Seasonal NO_3 loss (kg ha^{-1})
Bilevel	Base period	0.95	5.7	10.7
	RCP2.6	1.72	8.8	16.3
	RCP4.5	2.11	10.0	18.6
	RCP6.0	2.36	9.8	18.3
	RCP8.5	1.89	9.5	17.8
$D_{0.65}L_{15}$	Base period	0.95	4.8	18.0
	RCP2.6	1.54	5.7	21.3
	RCP4.5	1.60	6.0	22.3
	RCP6.0	1.66	5.8	21.7
	RCP8.5	1.54	5.7	21.3
$D_{0.65}L_{30}$	Base period	1.12	6.2	11.5
	RCP2.6	1.98	10.7	19.9
	RCP4.5	2.25	13.4	25.0
	RCP6.0	2.35	13.8	25.8
	RCP8.5	1.81	10.5	19.7
$D_{0.90}L_{30}$	Base period	2.61	13.3	24.8
	RCP2.6	2.94	13.8	25.8
	RCP4.5	3.50	17.0	31.7
	RCP6.0	3.71	17.6	32.9
	RCP8.5	2.93	14.4	26.9

installing costly drainage systems to mitigate further problems. An increase in P during seasons may also provide favorable conditions for the growth of weeds and pests and may enhance soil erosion, along with a considerable change in the soil available water (Enete and Amusa, 2010). Such consequences may reduce economic benefits by restraining the proper crop growth.

Fig. 7 shows that monthly ET_0 may slightly increase by 2.4–10.3 % throughout October-March. The highest increase can be observed in autumn during the October-December period. However, monthly ET_0 is likely to be reduced by 0.6 % and 2.3 % in April and May, respectively. Such a decrease can be a result of a small increase in monthly average T_{max} in the same period. The highest increase in ET_0 can be observed in autumn. Having a key role in the hydrological cycle, an increase in ET_0 may threaten agricultural sustainability since it may lead to a significant increase in the agricultural demand for water beyond its sustainable availability in a region. Such an increase may cause a significant reduction in water availability due to the overexploitation of surface and groundwater resources (Terink et al., 2013). Other researchers also support a projected increase in ET_0 in Iran (e.g., Terink et al., 2013; Karandish and Mousavi, 2018; Darzi-Naftchali and Karandish, 2019).

3.2.2. Drainage flux

Daily HYDRUS-simulated drainage fluxes for different drainage systems under future global warming projections (the ensemble average of 20 GCMs for each RCP scenario) are displayed in Fig. 8. While daily drain fluxes due to climate change projections both decreased and increased in different periods compared to the base scenario, they are more likely to increase, especially during the October-January period. Drainage fluxes are highly dependent on climatic variables, and particularly on P and ET_0. While an increase in ET_0 may lead to a likely reduction in drainage fluxes due to an increase in crop water uptake, this positive effect may be reversed by a negative impact of increased precipitation on q.

The results in Fig. 8 indicate that the monthly green water surplus (GWS), defined as $GWS = P\text{-}ET_0$ for a particular month (Karandish and Mousavi, 2018), will significantly increase due to global warming and a corresponding increase in monthly precipitation, which will consequently enhance drainage fluxes. Simulated drainage fluxes for different drainage systems seem to be more uncertain early in the simulation rather than later.

Based on the ensemble average of 20 GCMs for each RCP scenario, average drainage fluxes during the growing season were calculated for each drainage system, and the results are summarized in Table 4. Compared to the base period, the average drainage fluxes over the cropping cycle may increase by 112.3 % (80.6–148.3 %), 66.9 % (62.0–74.9 %), 87.5 % (61.8–110.2 %), and 25.1 % (12.0 %–42.1 %) for the Bilevel, $D_{0.65}L_{15}$, $D_{0.65}L_{30}$, and D0.90L30 drainage systems, respectively. For all drainage systems, the RCP6.5 scenario leads to the highest increase in the average drainage flux over the cropping cycle, while the RCP2.6 scenario leads to the lowest increase.

3.2.3. Nitrate flux

Daily HYDRUS-simulated NO_3 fluxes for different drainage systems under future global warming projections (the ensemble average of 20 GCMs for each RCP scenario) are displayed in Fig. 9. The visual inspection shows a dramatic increase in NO_3 fluxes during the October-January period when monthly precipitations are also relatively high. This pattern is also a consequence of increased drainage fluxes in these future climate scenarios (Fig. 9). Fig. 9 also shows that during the October-January period, the range of uncertainties arising from the projections of different RCPs is also higher than during the other periods. While the Bilevel and $D_{0.65}L_{30}$ drainage systems registered increased NO_3 fluxes during the entire growing cycle, the $D_{0.65}L_{15}$ and $D_{0.90}L_{30}$ drainage systems experienced a considerable decrease in NO_3 fluxes during the February-March period. More similar predicted NO_3 fluxes were obtained for all drainage systems during the February-March period, indicating less uncertainty during this time. Such results may be attributed to lower NO_3 soil concentrations during this period due to high crop N uptake during previous months (Darzi-Naftchali et al., 2017; DeDatta, 1981).

Based on the ensemble average of 20 GCMs for each RCP scenario, the minimum, maximum and average NO_3 fluxes during the growing season were calculated for each drainage system, and results are summarized in Table 4. The average NO_3 flux over the cropping cycle may increase by 53.3–74.8 %, 18.6–23.9 %, 71.3–124.9 %, and 4–32.6 % in the Bilevel, $D_{0.65}L_{15}$, $D_{0.65}L_{30}$, and $D_{0.90}L_{30}$ drainage systems, respectively. For all drainage systems, the RCP4.5 and RCP6.5 scenarios may result in the highest increase in the average NO_3 flux over the cropping cycle.

3.2.4. Seasonal nitrate losses

The seasonal NO_3 losses for different drainage systems were computed based on the ensemble average of 20 GCM projections for each RCP scenario (Table 4). Regardless of the time (i.e., either during the base or future periods), the lowest NO_3 loss always occurred for the $D_{0.65}L_{15}$ drainage system, where drains are installed at a shallower depth and at a smaller distance. On the other hand, the $D_{0.90}L_{30}$ drainage system always had the highest NO_3 losses during the growing seasons, indicating that NO_3 losses increase when drains are installed at deeper depths and larger distances (Cooke et al., 2002; Burchell, 2003; Yoon et al., 2006). These results indicate the importance of selecting a proper drainage system when sustainable agriculture and a safe environment are the primary concern.

Table 4 shows that climate change may result in higher seasonal NO_3 losses for all drainage systems. Compared to the base period, these increases will be 66.8 % (53.3–74.8 %), 20.5 % (18.6–23.9 %), 96.8 % (71.3–124.9 %), and 18.2 % (4–32.6 %) for the Bilevel, $D_{0.65}L_{15}$, $D_{0.65}L_{30}$, and $D_{0.90}L_{30}$ drainage systems, respectively. The lowest and the highest increases in NO_3 losses are expected to occur in the $D_{0.90}L_{30}$ and $D_{0.65}L_{30}$ drainage systems, respectively.

Increased NO_3 losses due to climate change may be attributed either to increased drain fluxes or the field management practices and, in particular, to the N-fertilization management. Drain fluxes can be controlled by various factors, including climatic variables, especially P and ET_0, soil hydraulic properties, the design of the drainage system,

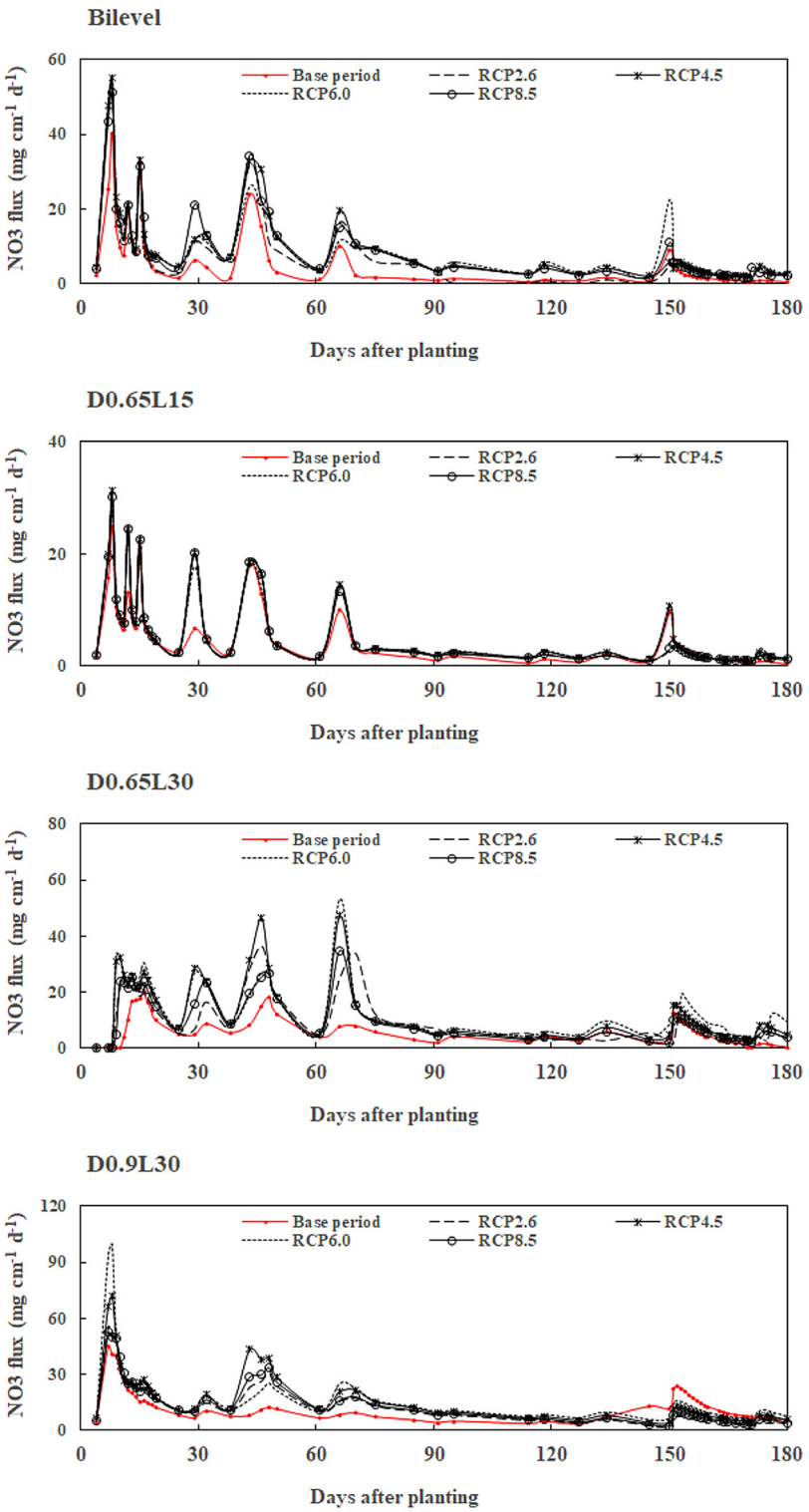

Fig. 9. Temporal variations of NO_3^- fluxes for different drainage systems (Bilevel, $D_{0.65}L_{15}$, $D_{0.65}L_{30}$, and $D_{0.90}L_{30}$) for the base period (1975-2005) and the 2041-2070 period for different RCPs.

and crop management. Hence, increased seasonal NO_3 losses may be partially attributed to increased drainage fluxes resulting from a profound increase in surplus precipitation (i.e., $P\text{-}ET_0$) due to global warming (Table 4). While future changes in climate variables may be inevitable, negative consequences of climate change projections on drain fluxes may be alleviated by improving the soil water holding capacity. Such improvements may be achieved by applying various organic amendments, such as manure or gypsum (Udayasoorian et al., 2009), organic mulches (Chukalla et al., 2015), or proper tillage practices (Liu et al., 2013). Organic mulching is also reported to have a positive effect on reducing nutrient leaching in agricultural lands (De Vita et al., 2007; Mitchell et al., 2012), and is commonly proposed as an effective measure to prevent water pollution under intensive agriculture (Azooz and Arshad, 1996; Triplett and Dick, 2008; Constantin et al., 2010; Chukalla et al., 2017). In particular, organic mulching may restrict N-leaching from the soil surface layer, where sufficiently high

concentrations of N enable continued uptake by roots (Phogat et al., 2013).

Drain depths and spacings also affect drain fluxes (Wahba and Christen, 2006). Jafari-Talukolaee et al. (2015) reported that increasing drain spacing might reduce drainage volumes in the subsurface-drained paddy field. The impact of installing either deep or shallow drainage systems on drainage water quality/quantity in Southern Australian irrigated lands was investigated by Christen and Skehan (2001). Their results demonstrated that lower drainage volumes occur from drainage systems with reduced drain depths and spacings. The long-term field investigation in the paddy field in northern Iran indicated that shallow drains were more effective than deeper ones in controlling the water table depth during the first three years after the installation of subsurface drainage while the reverse trend was observed in the fourth year (Jafari-Talukolaee et al., 2016). However, shallow drains may produce serious environmental problems since they enhance leaching and, consequently, may increase seasonal NO_3 losses (Darzi-Naftchali et al., 2017). Hence, drain depths and spacing need to be optimized depending on the main agricultural or environmental concerns and future global warming projections.

N-fertilization management is among the most crucial field practices, which significantly affect NO_3 losses. Numerous researchers demonstrated the close relationship between the N-fertilizer application rate/timing and N-leaching in agricultural lands (Mosier et al., 2002; Gasser et al., 2002; Haverkort et al., 2003; Daudén and Quilez, 2004; Alva et al., 2006; Barton and Colmer, 2006; Hutton et al., 2008; Wei et al., 2009; Jia et al., 2014; Karandish and Šimůnek, 2017). Besides, it is worth noting that the type of N-fertilizer can also affect the N-leaching rate (Jia et al., 2014). On the other hand, N is an essential crop nutrient, that profoundly affects crop growth and yield (Wienhold et al., 1995; Jia et al., 2014). An insufficient N supply in soil may result in severe yield and economic losses (Wienhold et al., 1995; Jia et a1., 2014). Therefore, further research should be carried out to find out the environmentally/economically safer applications of N-fertilizers under future global warming predictions.

4. Conclusion

Field experiments and modeling analyses involving a subsurface-drained field of rained-canola, as a winter crop, were carried out to evaluate the integrated influence of subsurface drainage and global warming on probable future water and N losses. Our quantitative assessment successfully evaluated the capability of the HYDRUS model to predict soil water contents, soil nitrate concentrations, and drainage/nitrate fluxes for various drainage systems. While the downscaled weather data from 20 GCMs and four RCP scenarios projected both decreases and increases in different future climatic variables, the ensemble averages predicted an increase in air temperatures, precipitation P, and potential evapotranspiration ET_0 for the 2041–2070 period. Surplus precipitation (defines as P-ET_0) is also likely to increase under climate change, which consequently resulted in a considerable increase in average values of drainage/nitrate fluxes during the growing season. Such increases may lead to an increase of 4–125 % in seasonal N losses for various drainage systems in the coming future. Our results demonstrate that negative environmental consequences of global warming, in terms of its effect on water and nitrate losses, may be alleviated when drains are installed at a shallow depth of 65 cm and at a spacing of 15 m ($D_{0.65}L_{15}$). Such a system should be more beneficial regarding either the water table control or reducing seasonal N losses from rainfed cropping systems. Based on our results, it can be concluded that achieving sustainable rainfed agriculture under global warming requires further serious attempts to identify the best field management practices aiming at diminishing environmental consequences.

Additionally, the HYDRUS model could be a proper alternative to the costly and labor/time-consuming field investigations to determine the optimal management scenarios in rainfed lands under global warming conditions. While simulating the effects of climate change projections on crop yield was not among the objectives of this research, such effects may be of high importance when economic interests are considered. Further research is thus needed to compare both economic and environmental consequences to obtain a full picture of the coming future.

Declaration of Competing Interest

The authors declare that they have no known competing financial interests or personal relationships that could have appeared to influence the work reported in this paper.

Acknowledgement

Fatemeh Karandish would like to appreciate the support of University of Zabol for carrying out this research under the grant number “UOZ_GR_9618_4”.

Appendix A. Supplementary data

Supplementary material related to this article can be found, in the online version, at doi:https://doi.org/10.1016/j.agwat.2020.106420.

References

Abbaspour, C.K., Faramarzi, M., Seyed Ghasemi, S., Yong, H., 2009. Assessing the impact of climate change on water resources in Iran. Water Res. 45, 1–16.
Adham, A., Wesseling, J.C., Abed, R., Riksen, M., Ouessar, M., Ritsema, C.J., 2019. Assessing the impact of climate change on rainwater harvesting in the Oum Zessar watershed in Southeastern Tunisia. Agric. Water Manag. 221, 131–140.
Agarwal, A., Babel, M.S., Maskey, Sh., 2014. Analysis of future precipitation in the Koshi river basin. Nepal. J. Hydrol. 513, 422–434.
Allen, R.G., Pereira, L.S., Raes, D., Smith, M., 1998. Crop evapotranspiration guidelines for computing crop water requirements. Irrigation and Drainage Paper 56, Rome, Italy. P.300.
Alva, A.K., Paramasivam, S., Obreza, T.A., Schumann, A.W., 2006. Nitrogen best management practice for citrus trees I. Fruit yield, quality, and leaf nutritional status. Sci Horti 107, 233–244.
Azooz, R., Arshad, M., 1996. Soil infiltration and hydraulic conductivity under long-term no-tillage and conventional tillage systems. Can. J. Soil Sci. 76, 143–152.
Barton, L., Colmer, T.D., 2006. Irrigation and fertilizer strategies for minimizing nitrogen leaching from turfgrass. Agric. Water Manage. 80, 160–175.
Bear, J., 1972. Dynamics of Fluid in Porous Media. Elsevier, New York, NY.
Burchell, M.R., 2003. Practices to Reduce Nitrate-nitrogen Losses from Drained Agricultural Lands. Phd Diss. North Carolina State University, Raleigh, N.C.
Burow, K.R., Nolan, B.T., Rupert, M.G., Dubrovsky, N.M., 2010. Nitrate in groundwater of the United States, 1991–2003. Environ. Sci. Technol. 44, 4988–4997.
CCSP, 2008. Climate models: an assessment of strengths and limitations. A Report by the U.S. Climate Change Science Program and the Subcommittee on Global Change Research. Department of Energy, Office of Biological and Environmental Research, Washington, D.C., USA p. 124.
Christen, E.W., Skehan, D., 2001. Design and management of subsurface horizontal drainage to reduce salt loads. J. Irrig. Drain. Eng. ASCE 127, 148–155.
Chukalla, A.D., Krol, M.S., Hoekstra, A.Y., 2015. Green and blue water footprint reduction in irrigated agriculture: effect of irrigation techniques, irrigation strategies and mulching. Hydrol. Earth Syst. Sci. 19 (12), 4877–4891.
Chukalla, A.D., Krol, M.S., Hoekstra, A.Y., 2017. Marginal cost curves for water footprint reduction in irrigated agriculture: guiding a cost-effective reduction of crop water consumption to a permit or benchmark level. Hydrol. Earth Syst. Sci. 21, 3507–3524.
Constantin, J., Mary, B., Laurent, F., Aubrion, G., Fontaine, A., Kerveillant, P., Beaudoin, N., 2010. Effects of catch crops, no till and reduced nitrogen fertilization on nitrogen leaching and balance in three long-term experiments. Agric. Ecosyst. Environ. 135, 268–278.
Cooke, R., Nehmelman, J., Kalita, P., 2002. Effect of tile depth on nitrate transport from tile drainage systems. ASAE Paper No. 022017.
Dahan, O., Babad, A., Lazarovitch, N., Russak, E.E., Kurtzman, D., 2014. Nitrate leaching from intensive organic farms to groundwater. Hydrol. Earth Syst. Sci. Discuss. 18, 333–341.
Darzi-Naftchali, A., Karandish, F., 2019. Adapting rice production to climate change for sustainable blue water consumption: an economic and virtual water analysis. Theor. Appl. Climatol. 135, 1–12.
Darzi-Naftchali, A., Ritzema, H., 2018. Integrating irrigation and drainage management to sustain agriculture in Northern Iran. Sustainability 10, 1775. https://doi.org/10.3390/su1006177.
Darzi-Naftchali, A., Mirlatifi, S.M., Shahnazari, A., Ejlali, F., Mahdian, M.H., 2013. Effect

of subsurface drainage on water balance and water table in poorly drained paddy fields. Agric. Water Manag. 130, 61–68.
Darzi-Naftchali, A., Shahnazari, A., Karandish, F., 2017. Nitrogen loss and its health risk in paddy fields under different drainage managements. Paddy Water Environ. 15, 145–157.
Darzi-Naftchali, A., Karandish, F., Šimůnek, J., 2018. Numerical modeling of soil water dynamics in subsurface drained paddies with the midseason drainage or alternate wetting and drying management. Agric. Water Manag. 197, 67–78.
Dastoorani, M.T., Poormohammadi, S., 2012. Evaluation of the effects of climate change on temperature, precipitation and evapotranspiration in Iran. In: International Conference on Applied Life Sciences. Turkey. pp. 73–79.
Daudén, A., Quilez, D., 2004. Pig slurry versus mineral fertilization on corn yield and nitrate leaching in a Mediterranean irrigated environment. Eur. J. Agron. 21, 7–19.
De Vita, P., Di Paolo, E., Fecondo, G., Di Fonzo, N., Pisante, M., 2007. No-tillage and conventional tillage effects on durum wheat yield, grain quality and soil moisture content in southern Italy. Soil Tillage Res. 92, 69–78.
DeDatta, S.K., 1981. Principles and Practices of Rice Production. IRRI, Los Bano ˜s, Philippines 618 pp.
Dudley, L.M., Ben-Gal, A., Lazarovitch, N., 2008. Drainage water reuse: biological, physical, and technological considerations for system management. J. Environ. Qual. 37, 25–35.
Enete, A.A., Amusa, T.A., 2010. Challenges of Agricultural Adaptation to Climate Change in Nigeria: a Synthesis from the Literature», Field Actions Science Reports [Online]. URL:. . http://factsreports.revues.org/678.
Filipovic, V., Mallmann, F.J.K., Coquet, Y., Šimůnek, J., 2014. Numerical simulation of water éfi in tile and mole drainage systems. Agric. Water Manag. 146, 105–114.
Furukawa, Y., Shiratori, Y., Inubushi, K., 2008. Depression of methane productionpotential in paddy soils by subsurface drainage systems. Soil Sci. Plant Nutr. 54, 950L–959L.
Gasser, M.O., Laverdiere, M.R., Lagace, Caron R.J., 2002. Impact of potato-cereal rotation and slurry applications on nitrate leaching and nitrogen balance in sandy soils. Can. J. Soil Sci. 82, 469–479.
Girvetz, E.H., Zganjar, C., Raber, G.T., Maurer, E.P., Kareiva, P., 2009. Applied climate-change analysis: the climate wizard tool. PLoS One 4 (12), e8320. https://doi.org/10.1371/journal.pone.0008320.
Haj-Amor, Z., Acharhee, T.K., Dhaouadi, L., Bouri, S., 2020. Impacts of climate change on irrigation water requirement of date palms under future salinity tren in coastal aquifer of Tunisian oasis. Agric. Water Manag. 228, 105843.
Hanson, B.R., Šimůnek, J., Hopmans, J.W., 2006. Evaluation of urea-ammonium-nitrate fertigation with drip irrigation using numerical modeling. Agric. Water Manag 86, 102–113.
Harmsen, E.W., Miller, N., Schlegel, N.J., Gonzalez, J.E., 2009. Seasonal climate change impacts on evapotranspiration, precipitation éficit and yield in Puerto Rico. Agric. Water Manag. 96, 1085–1095.
Haverkort, A.J., Vos, J., Booij, R., 2003. Precision management of nitrogen and water in potato production through monitoring and modeling. In: Proceedings of the XXVI International Horticultural Congress: Potatoes, Healthy Food for Humanity: International Developments in Breeding, Production, Protection and Utilization. Toronto, Canada.
Hoekstra, A.Y., Mekonnen, M.M., Chapagain, A.K., Mathews, R.E., Richter, B.D., 2012. Global monthly water scarcity: blue water footprints versus blue water availability. PlosOne 7 (2), e32688.
Hutton, R., Holzapfel, B., Smith, J., Hutchinson, P., Barlow, K., Bond, W., 2008. Influence of irrigation and fertilizer management on the movement of water and nutrients within and below rootzone of vines for sustainable grape production. CRC for Viticulture Report S2.3.6.
IPCC, 2013. Climate change 2013: the physical science basis. In: Stocker, T.F., Qin, D., Plattner, G.-K., Tignor, M., Allen, S.K., Boschung, J., Nauels, A., Xia, Y., Bex, V., Midgley, P.M. (Eds.), Contribution of Working Group I to the Fifth Assessment Report of the Intergovernmental Panel on Climate Change. Cambridge University Press, Cambridge, United Kingdom and New York, NY, USA 1535 pp.
Jafari-Talukolaee, M., Shahnazari, A., Ahmadi, Z.M., Darzi-Naftchali, A., 2015. Drain discharge and salt load in response to subsurface drain depth and spacing in paddy fields. J. Irrig. Drain. Eng. 141 (11), 1–6 04015017.
Jafari-Talukolaee, M., Ritzema, H., Darzi-Naftchali, A., Shahnazari, A., 2016. Subsurface drainage to enable the cultivation of winter crops in consolidated paddy fields in northern Iran. Sustainability 8 (249), 1–19.
Jia, X., Shao, L., Liu, P., Zhao, B., Gu, L., Dong, Sh., Bing, S.H., Zhang, J., Zhao, B., 2014. Effect of different nitrogen and irrigation treatments on yield and nitrate leaching of summer maize (Zea mays L.) under lysimeter conditions. Agric. Water Manage. 137, 92–103.
Jones, P.D., Osborn, T.J., Briffa, K.R., 1997. Estimating sampling errors in large-scale temperature averages. J. Clim. 10 (10), 2548–2568.
Kalita, P.K., Algoazany, A.S., Mitchell, J.K., Cooke, R.A.C., Hirschi, M.C., 2006. Subsurface water quality from a flat tile-drained watershed in Illinois, USA. Agric. Ecosyst. Environ. 115, 183–193.
Kandelous, M.M., Kamai, T., Vrugt, J.A., Šimůnek, J., Hanson, B., Hopmans, J.W., 2012. Evaluation of subsurface drip irrigation design and management parameters for alfalfa. Agric. Water Manag. 109, 81–93.
Karandish, F., Mousavi, S.S., 2018. Climate change uncertainty and risk assessment in Iran during 21th century: evapotranspiration and green water deficit analysis. Theor. Appl. Climatol. 131 (1–2), 777–791.
Karandish, F., Šimůnek, J., 2016. A field-modeling study for assessing temporal variations of soil-water-crop interactions under water-saving irrigation strategies. Agric. Water Manag. 178, 291–303.
Karandish, F., Šimůnek, J., 2017. Two-dimensional modeling of nitrogen and water dynamics for various N-managed water-saving irrigation strategies using HYDRUS. Agric. Water Manag. 193, 174–190.
Karandish, F., Kalanaki, M., Saberali, S.F., 2016. Projected impacts of global warming on cropping calendar and water requirement of maize in a humid climate. Arch. Agron. Soil Sci. 63 (1), 1–13.
Karandish, F., Mousavi, S.S., Tabari, H., 2017. Climate change impact on precipitation and cardinal temperatures in different climatic zones in Iran: analyzing the probable effects on cereal water-use efficiency. Stoch. Environ. Res. Risk Assess. 31, 2121–2146. https://doi.org/10.1007/s00477-016-1355-y.
Kazemi-Rad, L., Mohammadi, H., 2015. Climate change assessment in Gilan Province. Iran. Int. J. Agric. Crop. Sci. 8 (2), 86–93.
Li, H., Han, Y., Cai, Z., 2003. Nitrogen mineralization in paddy soils of the Taihu Region of China under anaerobic conditions: dynamics and model fitting. Geoderma 115, 161–175.
Li, Y., Šimůnek, J., Jing, L., Zhang, Z., Ni, L., 2014. Evaluation of water movement and water losses in a direct-seeded-rice field experiment using HYDRUS-1D. Agric. Water Manag. 142, 38–46.
Liu, Y., Gao, M., Wu, W., Tanweer, S.T., Wen, X., Liao, Y., 2013. The effects of conservation tillage practices on the soil water-holding capacity of a non-irrigated apple orchard in the Loess Plateau, China. Soil Tillage Res. 130, 7–12.
Massah Bavani, A.R., Morid, S., 2005. Risk Assessment of Climate Change and Its Impact on Water Resources. PhD Thesis. Tarbiat Modares University.
Matteau, J.P., Gumiere, S.J., Gallichand, J., Letourneau, G., Khiari, L., Gasser, M.O., Michaud, A., 2019. Coupling of a nitrate production model with HYDRUS to predict nitrate leaching. Agric. Water Manag. 213, 616–626.
Mekala, C., Nambi, I.M., 2016. Experimental and simulation studies on Nitrogen dynamics in unsaturated and saturated soil using HYDRUS-2D. Procedia Technol. 25, 122–129.
Mguidiche, A., Provenzano, G., Douh, B., Khila, S., Rallo, G., Boujelben, A., 2015. Assessing HYDRUS-2D to simulate soil water content (SWC) and salt accumulation under an SDI system: application to a potato crop in a semi-arid area of central Tunisia. Irrig. Drain. 64, 263–274.
Mirjat, M.S., Mughal, A.Q., Chandio, A.S., 2014. Simulating water flow and salt leaching under sequential flooding between subsurface drains. Irrig. Drain. 63, 112–122.
Mitchell, J., Singh, P., Wallender, W., Munk, D., Wroble, J., Horwath, W., Hogan, P., Roy, R., Hanson, B., 2012. No-tillage and high-residue practices reduce soil water evaporation. Calif. Agric. 66, 55–61.
Mosier, A.R., Bleken, M.A., Chaiwanakupt, P., Ellis, E.C., Freney, J.R., Howarth, R.B., Matson, P.A., Minami, K., Naylor, R., Weeks, K.N., Zhu, Z.L., 2002. Policy implications of human-accelerated nitrogen cycling. Biogeochemistry 57, 477–516.
Öztekin, T., 2002. Simulating water flow to a subsurface drain in a layered soil. Turk. J. Agric. For. 26, 179–185.
Phogat, V., Skewes, M.A., Cox, G., Alam, J., Grigson, G., Šimůnek, J., 2013. Evaluation of water movement and nitrate dynamics in a lysimeter planted with an orange tree. Agric. Water Manage. 127, 74–84.
Radcliffe, D., Šimůnek, J., 2010. Soil Physics With HYDRUS: Modeling and Applications. CRC Press, Taylor & Francis Group, Boca Raton, FL ISBN: 978-1-4200-7380-5, pp. 373.
Ramos, T.B., Šimůnek, J., Goncalves, M.C., Martins, J.C., Prazeres, A., Pereira, L.S., 2012. Two-dimensional modeling of water and nitrogen fate from sweet sorghum irrigated with fresh and blended saline waters. Agric. Water Manag. 111, 87–104.
Randall, D.A., Wood, R.A., Bony, S., Colman, R., Fichefet, T., Fyfe, J., et al., 2007. Climate models and their evaluation. Climate Change 2007: The Physical Science Basis. Contribution of Working Group I to the ARIV of IPCC. Cambridge University Press, Cambridge, United Kingdom and New York, NY, USA.
Šimůnek, J., van Genuchten, M.Th., Šejna, M., 2008. Development and applications of the HYDRUS and STANMOD software packages and related codes. Vadose Zone J. 7 (2), 587–600. https://doi.org/10.2136/VZJ2007.0077.
Tafteh, A., Sepaskhah, A.R., 2012. Application of HYDRUS-1D model for simulating water and nitrate leaching from continuous and alternate furrow irrigated rapeseed and maize fields. Agric. Water Manage. 113, 19–29.
Terink, W., Immerzeel, W.W., Droogers, P., 2013. Climate change projections of precipitation and reference evapotranspiration for the Middle East and Northern Africa until 2050. Int. J. Climatol. 33, 3055–3072. https://doi.org/10.1002/joc.3650.
Thompson, A.J., Andrews, J., Mulholland, B.J., McKee, J.M.T., Hilton, H.W., Horridge, J.S., Farquhar, G.D., Smeeton, R.C., Smillie, I.R.A., Black, C.R., Taylor, I.B., 2007. Overproduction of Abscisic acid in tomato increases transpiration efficiency and root hydraulic conductivity and influences leaf expansion. Plant Physiol. 143, 1905–1917.
Triplett, G., Dick, W.A., 2008. No-tillage crop production: a revolution in agriculture!. Agron. J. 100, S-153–S-165.
Trzaska, S., Schnarr, E., 2014. A Review of Downscaling Methods for Climate Change Projections. USAID 56p.
Udayasoorian, C., Sebastian, S.P., Jayabalakrishnan, R.M., 2009. Effect of amendments on problem soils with poor quality irrigation water under sugarcane crop. Am.-Eurasian J. Agric. And Environ. Sci. 5, 618–626.
Van Genuchten, M.T., 1980. A closed-form equation for predicting the hydraulic conductivity of unsaturated soils. Soil Sci. Soc. Am. J. 44, 892–898.
Wahba, M.A.S., Christen, E.W., 2006. Modeling subsurface drainage for salt load management in southeastern Australia. Irrig. Drain. Syst. J. 20, 267–282.
Wang, H., Ju, X., Wei, Y., Li, B., Zhao, L., Hu, K., 2010. Simulation of bromide and nitrate leaching under heavy rainfall and high-intensity irrigation rates in North China Plain. Agric. Water Manag. 97, 1646–1654.
Wei, Y.P., Chen, D.L., Hu, K.L., Willett, I.R., Langford, J., 2009. Policy incentives for reducing nitrate leaching from intensive agriculture in desert oases of Alxa, InnerMongolia, China. Agr Water Manage 96, 1114–1119.
Wienhold, B.J., Trooien, T.P., Reichman, G.A., 1995. Yield and nitrogen use efficiency of

irrigated corn in the northern Great Plains. Agron. J. 87 (5), 842–846.
Wijanarko, A., 2015. Effect of organic matter and soil fertility on nitrogen mineralization and uptake by Cassava (Manihot esculenta Crantz) in a typic hapludults. J Exp Biol Agric Sci. 3 (3), 232–240.
WWAP, 2009. World Water Assessment Programme: the UN World Water Development Report 3: Water in a Changing World. UNESCO, Paris, France, Earthscan, London, UK.
Yoon, K.S., Choi, J.K., Son, J.G., Cho, J.Y., 2006. Concentration profile of nitrogen and phosphorus in leachate of a paddy plot during the rice cultivation period in southern Korea. Commun. Soil Sci. Plant Anal. 37, 1957–1972.
Zhang, Q., Jimenez, J.L., Canagaratna, M.R., 2007. Ubiquity and dominance of oxygenated species in organic aerosols in anthropogenically-influenced Northern Hemisphere midlatitudes. Geophys. Res. Lett. 34, L13801.
Zhu, J.H., Li, X.L., Christie, P., Li, J.L., 2005. Environmental implications of low nitrogen use efficiency in excessively fertilized hot pepper (Capsicum frutescens L.) cropping systems. Agric. Ecosyst. Environ. 111, 70–80.
Zickfeld, K., Knopf, B., Petoukhov, V., Schellnhuber, H.J., 2005. Is the Indian summer monsoon stable against global change? Geophys. Res. Lett. 32, L15707.